



534229

**AIAA 94-1854**

**Wind Tunnel Results of Pneumatic  
Forebody Vortex Control using  
Rectangular Slots on a Chined  
Forebody**



Captain Michael Alexander  
Flight Dynamics Directorate  
Wright-Patterson AFB, OH

Larry A. Meyn  
NASA Ames Research Center  
Moffett Field, CA

**AIAA 12th Applied Aerodynamics Conference**  
June 20-23, 1994/ Colorado Springs, CO



# Wind Tunnel Results of Pneumatic Forebody Vortex Control using Rectangular Slots on a Chined Forebody

Michael G. Alexander<sup>†</sup>  
Flight Dynamics Directorate  
Wright-Patterson AFB, Ohio

Larry A. Meyn<sup>‡</sup>  
NASA-Ames Research Center  
Moffett Field, California

## Abstract

A subsonic wind tunnel investigation of pneumatic vortex flow control on a chined forebody using slots was accomplished at a dynamic pressure of 50 psf resulting in a  $R_n/ft$  of  $1.3 \times 10^6$ . Data were acquired from angles of attack ranging from  $-4^\circ$  to  $+34^\circ$  at side slips of  $+0.4^\circ$  and  $+10.4^\circ$ . The test article used in this study was the 10% scale Fighter Lift and Control (FLAC) advanced diamond winged, vee-tailed fighter configuration. Three different slot blowing concepts were evaluated; outward, downward, and tangential with all blowing accomplished asymmetrically. The results of three different mass flows (0.067, 0.13, and 0.26 lbm/s;  $C_\mu$ 's of  $\leq 0.006$ , 0.011, and 0.022 respectively) were analyzed and reported. Test data are presented on the effects of mass flows, slot lengths and positions and blowing concepts on yawing moment and side force generation.

Results from this study indicate that the outward and downward blowing slots developed yawing moment and side force increments in the direction opposite of the blowing side while the tangential blowing slots generated yawing moment and side force increments in the direction towards the blowing side. The outward and downward blowing slots typically produced positive pitching moment increments while the tangential blowing slots typically generated negative pitching moment increments. The slot blowing nearest the forebody apex was most effective at generating the largest increments and as the slot was moved aft or increased in length, its effectiveness at generating forces and moments diminished.

## Nomenclature

A	slot exit area, in <sup>2</sup>
C	orifice meter discharge coefficient, 0.63104
$\Delta C_l$	incremental rolling moment coefficient
$\Delta C_m$	incremental pitching moment coefficient
$\Delta C_n$	incremental yawing moment coefficient
$\Delta C_y$	incremental side force coefficient

<sup>†</sup> Aerospace Engineer.

<sup>‡</sup> Aerospace Engineer, Member AIAA

This paper is declared a work of the U.S. Government and is not subject to copyright protection in the United States.

$C_\mu$	blowing coefficient
D1	orifice meter pipe diameter, 2.067 in
D2	orifice diameter, 1.24 in
FLAC	Fighter Lift and Control
FVC	Forebody Vortex Control
Fa	thermal expansion factor, 1.0
g	gravitational constant, 32.1741 ft/sec <sup>2</sup>
LEF	leading edge flap
LEX	leading edge extension
LHS	left hand side
$\dot{m}$	mass flow, lbm/sec
M	Mach number
MAC	mean aerodynamic chord, ft
P <sub>1</sub>	orifice meter inlet pressure, psia
P <sub>s</sub>	static pressure, psia
q	free-stream dynamic pressure, psf
R	characteristic gas constant, 53.35 ft-lbf/lbm-°R
$R_n/ft$	Reynolds number per foot
RHS	right hand side
SCFM	standard cubic flow measurement
SWFP	static weight flow parameter
T <sub>1</sub>	orifice meter inlet temperature, °R
T <sub>s</sub>	static temperature, °R
T <sub>t</sub>	total temperature, °R
TEF	trailing edge flap
V <sub>j</sub>	velocity at slot exit, ft/sec
Z <sub>1</sub>	compressibility factor, 1.0
$\alpha$	angle of attack, deg
$\eta$	diameter ratio, D1/D2
$\beta$	angle of side slip, deg
$\Delta P$	pressure drop across orifice meter, psia
$\gamma$	specific heat ratio, 1.4

## Introduction

Modern and advanced fighter aircraft are required to operate in a flight regime that requires the maximum maneuverability and controllability possible in order to be effective in the combat arena. However, as geometries emerge that have been designed with a low observable requirement, they typically pay an aerodynamic penalty that usually results in the degradation of aircraft maneuver performance. Requirements for high maneuverability necessarily dictate that aircraft must fly at high angles of attack where the aerodynamics are dominated by separated and vortical flows. These flows can induce adverse,

highly-nonlinear longitudinal and lateral-directional control characteristics such as wing rock, loss of yaw and roll control, and uncontrolled pitch-up and deep stall. One brute force method to help overcome these nonlinear effects has been the use of thrust vectoring. Instead of trying to overcome the moments induced by various vortices, perhaps a more effective way to control the nonlinear effects and enhance aircraft controllability during an aggressive maneuver is by directly employing the shed vortices as an alternative source of high angle of attack control.

Innovative control augmentation devices that are effective at maneuver angles of attack are needed to supplement the aerodynamic control surfaces in returning and enhancing controllability for these advanced fighter aircraft configurations. One type of a vortex flow control augmentation concept that exhibited great potential is pneumatic forebody blowing. A large pneumatic blowing database<sup>1</sup> has been generated on circular and elliptical type forebodies and has shown this concept can generate significant amount of yaw power at maneuver angles of attack. One proven pneumatic concept has already been flight tested on the X-29A aircraft<sup>2</sup>. However, very little information exists on control augmentation of advanced fighter aircraft with chined forebodies. The Fighter Lift and Control (FLAC) program is one such program dedicated to investigating those innovative control devices that enhance the maneuver performance of advanced, low observable class fighter aircraft. The FLAC program is a cooperative program between the USAF Wright Laboratory and NASA-Ames Research Center and involves a series of experimental and computational investigations up to flight Reynolds numbers.

### Test Facility

The 10% FLAC model was tested in NASA-Ames' 7x10 foot subsonic atmospheric wind tunnel. Its test section is capable of a dynamic pressure ranging of 5 to 200 lbf/ft<sup>2</sup> and has the capability of delivering high pressure air up to 3,000 psi at flow rates up to 2,000 SCFM. A 800-kW heater system is available for heating the air up to 600°F.

The FLAC model was mounted in the tunnel using a floor supported sting mounted to a turntable that provided angles of attack. A 2.5-in diameter internal Task balance was used to acquire all forces and moments. Positive sideslip was achieved by introducing an appropriate angled wedge (+10°) between the top of the vertical sting support shaft and the sting.

### Model Description

The Fighter Lift and Control model used for this research is a 10% scaled configuration of a near term technology derivative, multi-role fighter concept

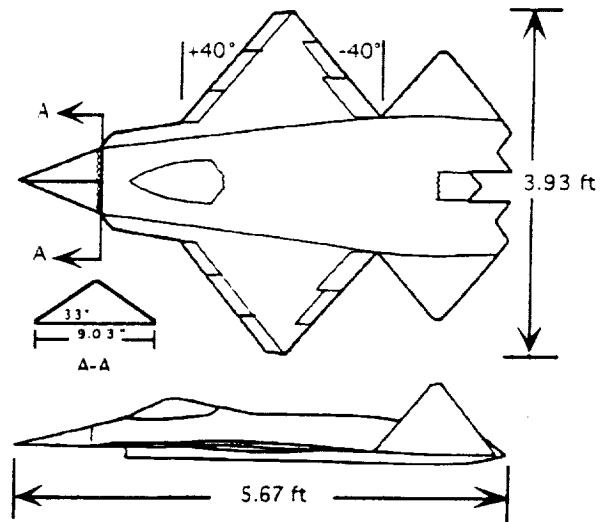


Figure 1 FLAC Configuration

that originated from ASC/XP, Innovative Concepts Branch, Wright-Patterson AFB, and can be seen in Figure 1. This configuration has a chined forebody, leading edge extension (LEX), deflectable leading and trailing edge flaps and vee-tails canted 45° from the horizontal plane, and a flow through inlet. The fuselage is 5.67 ft long and has a wing span of 3.93 ft with a wing reference area and aspect ratio of 7.302 ft<sup>2</sup> and 2.11 respectively. The wing leading and trailing edge sweep angle is ±40°. The wing leading edge flaps (LEF) are split into three equal segments and can be individually deflected from 0° to +45°. The inboard trailing edge flap is capable of deflecting 0° to +40° with the outboard trailing edge flap (aileron) capable of deflecting -30° to +40°. A 2mm-wide, #70-grit boundary layer trip strip was applied at 10% of the local chord on the upper and lower surfaces of the wings and tails. This model was designed and fabricated by Micro Craft Inc., Tullahoma, Tn.

### Pneumatic Forebody Description

The FLAC forebody (Figure 2) is a plenum capable of accepting multiple slotted nozzle types (outward, downward, tangential) and has the capability of symmetric or asymmetric blowing. The pneumatic forebody has a fineness ratio of 1.24 and has two internal porous-baffle plates located within the plenum

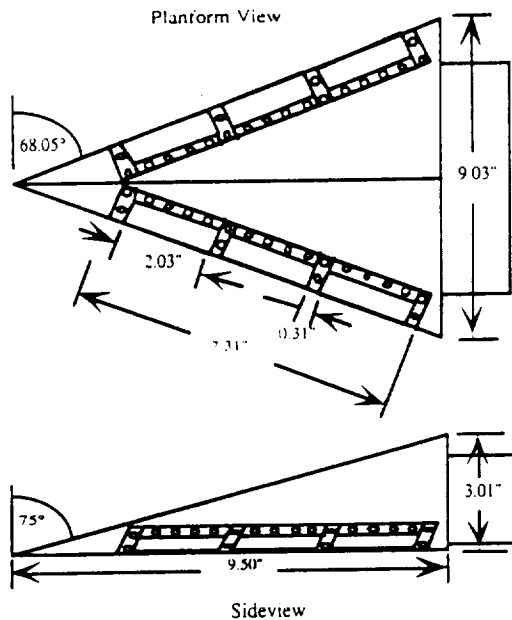


Figure 2 Pneumatic Forebody

which are used to attenuate most of the supply air jet momentum. Air was supplied to the forebody plenum via two 0.5-inch-diameter highly flexible, corrugated, braided stainless steel hoses.

### Slotted Nozzle Description

Three nozzle types were fabricated, outward, downward, and tangential; all three can be seen in Figure 3. Each nozzle is 7.31 inches long and divided into upper and lower halves and segmented into three slots of 2.03 inches in length by 0.031 inch in width at the exit with an exit area of 0.061 in<sup>2</sup>.

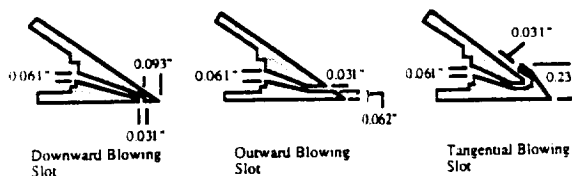


Figure 3 Slotted Nozzle Types

The slot segments could be opened or closed independently to evaluate slot lengths and position effects.

### Test Conditions

Test section dynamic pressure was 50 psf which resulted in a  $R_{\eta}/ft$  of  $1.3 \times 10^6$ . Data were acquired at angles of attack ranging from  $-4^\circ$  to  $+34^\circ$  and at sideslips of  $+0.4^\circ$  and  $+10.4^\circ$ . All slot blowing accomplished in this investigation was tails off with

asymmetric blowing with  $V_{jet}$  exiting from the left hand side or leeward side of the forebody. The leading and trailing edge flaps (including aileron) were set at a quasi-maneuver deflection of  $+10^\circ$ .

### Data Reduction

Data are presented as incremental data in the body axis system. Moments are referenced to 35 percent of the MAC with all aerodynamic data corrected for base and cavity drag and pressure tares but not for model blockage and pneumatic induced thrust effects.

### Mass Flow Determination

The mass flow rate was measured with an in-line orifice meter. Equations 2 through 4 (reference 4) were used to determine the mass flow rate. The thermal expansion factor,  $F_a$ , was set to 1.0 and is accurate to within  $\pm 0.5\%$  for temperatures from  $-400^\circ\text{F}$  to  $375^\circ\text{F}$ . The compressibility factor,  $Z$ , was set to 1.0 and is accurate to within  $\pm 1.0\%$  for temperatures from  $60^\circ\text{F}$  to  $300^\circ\text{F}$  and for pressures less than 500 psia.

$$\rho_1 = \frac{144 \cdot P_1}{Z_1 R T_1} \quad (\text{lb}_m/\text{ft}^3) \quad (2)$$

$$\gamma = 1 - \left(0.41 + 0.35\eta^4\right) \frac{\Delta P}{\gamma P_1} \quad (3)$$

$$\dot{m} = 0.52502 \left[ \frac{C Y D_2^2 F_a}{\sqrt{1 - \eta^4}} \right] \sqrt{\rho_1 \Delta P} \quad (\text{lb}_m/\text{sec}) \quad (4)$$

### Nozzle Exit Conditions

Nozzle exit conditions are determined by measuring total pressure and temperature in a plenum upstream of the nozzle and calculating the exit conditions from isentropic flow equations. Once the mass flow rate was found (equation 4), the exit Mach number was determined using the following continuity relationship from equation 5 (reference 5):

$$\text{SWFP} = \frac{\dot{m} \sqrt{T_t}}{P_s A} = M \left[ \frac{\gamma \gamma}{R} \left( 1 + \frac{\gamma - 1}{2} M^2 \right) \right]^{\frac{1}{2}} \quad (5)$$

The term on the left side of the equation is the static weight flow parameter,  $\text{SWFP}$ , that is determined from the mass flow rate,  $\dot{m}$ , the supply air total temperature,  $T_t$ , the wind tunnel static pressure,  $P_s$ , and the slot exit area,  $A$ . To simplify the determination of Mach number from the above relation, tabulated values of  $\text{SWFP}$  for Mach numbers ranging from 0 to 1 were curvefit to provide the following equation:

$$M = 1.0979 SWFP - 0.054357 SWFP^2 - 0.049577 SWFP^3 \quad (6)$$

SWFP is 1.0065 for a Mach number of 1. For values of SWFP greater than this the exit flow is assumed to be choked and the Mach number is set to 1. The static temperature,  $T_s$ , jet exit velocity,  $V_j$ , and the blowing coefficient,  $C_{\mu}$ , are determined from equations 7, 8, and 9 respectively.

$$T_s = \frac{T_i}{1 + \frac{\gamma - 1}{2} M^2} \quad (7)$$

$$V_j = M(\gamma R T_s)^{1/2} \quad (8)$$

$$C_{\mu} = \frac{m V_j}{q S_{ref} g} \quad (9)$$

### Chine Blowing

The maneuver aerodynamics of chined forebodies are characterized by fixing the separation location of the forebody vortices. These fixed separations on chine forebodies may limit the usefulness of control techniques that have proven successful on circular or elliptical forebodies. The natural vortex separation off the upper surface of a rounded forebody cross-section is frequently unstable and, as a result, highly susceptible to manipulation with very small inputs from mechanical or pneumatic methods. Since chined forebody separation points are fixed, they typically develop very energetic vortex structures that resist displacement<sup>3</sup> and will not react to fluidic switching. As a consequence, the vortex must be physically displaced off the chine edge. Consequently, manipulation techniques that result in high levels of force and moment generation for a limited input on conventional forebodies may have little or no effect on chined forebodies.

In this experimental effort, slot blowing was the nozzle of preference. Three proposed slotted pneumatic approaches to deal with a chined flow field were investigated. One approach was to force or displace the vortex off the chine edge and rely on the opposing chine vortex suction to produce asymmetric forces and moments. This approach was attempted with outward slot blowing. The second approach was to delay the formation or significantly displace the vortex core of a chine vortex. This is achieved by generating a jet sheet that simulates a fluidic dam or physical barrier that interrupts the vortex feeding sheet or displaces the vortex core of the chine vortex, while allowing the opposing vortex to form and generate asymmetric forces and moments opposite the blowing side. This approach was attempted with the downward slot blowing. The third and final approach was to lower the surface pressure on the forebody by blowing across it,

thus drawing in the chine vortex core next to the forebody surface via entrainment. By generating a larger suction flow field on the forebody on the blowing side, it allowed the force and moment increments to be generated on the blowing side. This approach was attempted with the tangential slot blowing.

## Results

### Outward Slot Blowing

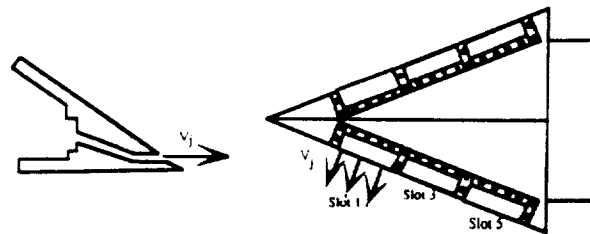


Figure 4 Outward Slot Blowing

Outward slot blowing is illustrated in Figure 4 above. As seen in Figures 4a and 4b, all outward blowing slots generate positive yawing moment increments (direction away from the blowing side) and are independent of sideslip. A slot position and length effect is observed in the outward blowing slots. The slot positioned nearest the forebody apex (slot 1) typically generates the largest yawing moment increments with the slot positioned furthest away from the apex (slot 5) generating a substantially smaller increment. As the slot length is increased (e.g. slot 1 to slot 1-3 or 1-3-5), the yawing moment generation capability diminishes. Observe the low angle of attack effectiveness at generating yawing moment increments. It appears that outward slot blowing might offer control augmentation at low angles of attack. Generally, a sideslip effect is observed which appears to enhance the slot performance in terms of generating larger force and moment increments; however, it is not recognized that slot effectiveness is enhanced inasmuch as the forebody vortex on the leeward side is stronger when compared to the vortex on the windward side. This apparent increase in vortex strength is attributed to the forebody planform angle on the leeward side increasing commensurate with increasing sideslip. In Figures 4a and 4b, it is apparent that slot 1 generates the largest yawing moment increments over a larger angle of attack range therefore, only its  $C_{\mu}$  effects (Figure 4c) are shown. As  $C_{\mu}$  is increased, the incremental yawing moment generation of slot 1 increases.

In the side force increments (Figure 4d and 4e), an angle of attack effect is observed. At  $\alpha < 8^\circ$  ( $\beta = +0.4^\circ$ ), all slots, except slot 1, generate diminishing positive (direction away from the blowing side) side force increments. By  $\alpha > 14^\circ$ , all slots (except slot 1) are generating negative increments. Each slot exhibits a

slope reversal with  $\alpha_{\text{reversal}}$  dependent upon slot length and position. By  $\alpha = 34^\circ$  (Figure 4d), all slots again are producing positive side force increments. Slot 1 at all angles of attack generates positive side force increments. The same slope reversal trend as seen in  $\beta = +0.4^\circ$  (Figure 4d) is observed at sideslip,  $\beta = +10.4^\circ$ , (Figure 4e) with the exception that all slots now generate positive increments at all angles of attack. Note at  $\alpha = 26^\circ$  slot 1 exhibits a rapid increase in positive side force increments. It is conjectured that slot 1 is responding to a center of pressure shift due to vortex bursting. Slot 1  $C_{\mu}$  effects at  $\beta = 0.4^\circ$  are shown in Figure 4f for constancy.

In Figures 4g and 4h, a slot length and position effect is observed in the pitching moment increments which are independent of sideslip. As the slot position is moved aft or increases in length, the slots generate positive (destabilizing) pitching moment increments with the exception of slot 1 which generates negative (stabilizing) increments. Note the sideslip effect particularly in slot 1. At  $\beta = +0.4^\circ$ , ( $\alpha > 24^\circ$ ), slot 1 changes slope and generates positive pitching moment increments while at  $\beta = +10.4^\circ$  ( $\alpha > 28^\circ$ ), all slots change slopes and produce negative pitching moment increments.

### Downward Slot Blowing

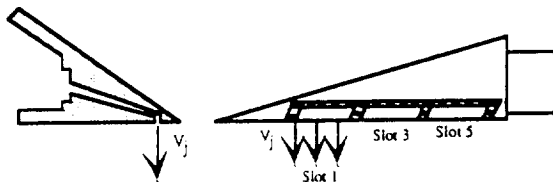


Figure 5 Downward Slot Blowing

The downward blowing slot is illustrated in Figure 5 above. As seen in Figures 5a and 5b, all downward blowing slots at  $\alpha \geq 15^\circ$  generate positive yawing moment increments (direction away from the blowing side), with the exception of slot 1-3, which are independent of sideslip, slot length, and angle of attack. Observe in Figures 5a, b, and c at  $\alpha < 15^\circ$  the angle of attack delay in the generation of a significant yawing moment increment. This angle of attack delay ( $\alpha_{\text{delay}}$ ) is due to the lack of a forebody vortex forming at those small angles and to the lack of an induced thrust effect. A sideslip effect is seen in Figures 5a and 5b in  $\alpha_{\text{delay}}$ . Even though all slots will eventually produce positive yawing moment increments, increasing the sideslip decreases the angle of attack ( $\alpha_{\text{delay}}$ ) where the positive increment begins. Since the forebody planform angle has increased from  $68^\circ$  to  $78.4^\circ$ , it is conjectured this decrease in angle of attack where the positive increment begins is primarily due to the development of the leeward vortex at  $\beta = +10.4^\circ$  at lower angles of attack. Note in Figure 5a ( $\beta = +0.4^\circ$ ) at  $\alpha > 15^\circ$  how the

yawing moment increments' trend seems to indicate a continually increasing positive yawing moment. But, in Figure 5b ( $\beta = +10.4^\circ$ ) at  $\alpha \geq 12^\circ$ , the yawing moment increments attain a nominal maximum positive increment with that maximum yawing moment shifting with slot length. But, once a maximum yawing moment is attained (Figure 5b), the yawing moment increments diminishes in magnitude over the angle of attack range and generally maintains a constant positive increment at  $\alpha \geq 28^\circ$ . Since slot 1 appears to offer the largest yawing moment increments over a larger angle of attack range, only its  $C_{\mu}$  effects (Figure 5c) are shown. As  $C_{\mu}$  is increased, the incremental yawing moment generation of slot 1 increases.

At low angles of attack, the side force increments typically begin with a negative magnitude which is independent of mass flow, sideslip and angle of attack (Figures 5d, e, and f). As seen in the yawing moment increments, a sideslip effect is observed in the shifting of the angle of attack where the side force increments range from negative to positive (Figure 5d and 5e). At  $\beta = +0.4^\circ$  (Figure 5d), the increments typically are negative up to  $\alpha \approx 20^\circ$ . While at  $\beta = +10.4^\circ$  (Figure 5e) at  $\alpha \leq 12^\circ$ , the side force increments are negative. This effect is conjectured to be due to the increased forebody sweep angle noted above. As the angle of attack is increased from  $\alpha_{\text{delay}}$ , all slots generate positive side force increments (direction opposite the blowing side). A slot length effect is seen with the shortest length nearest the forebody apex (slot 1) generating the largest positive side force increments. Increasing the slot length, diminishes the yawing moment generation capability of the slots. Slot 1  $C_{\mu}$  effects at  $\beta = +0.4^\circ$  are shown in Figure 5f for constancy.

In Figure 5g and 5h at  $\alpha < 15^\circ$ , a slot length effect is observed in the pitching moment increments which are independent of sideslip. It is observed that the shorter the slot length, the greater the positive (destabilizing) magnitude of the pitching moment increments. Also contributing to the positive pitching moment increments is the induced thrust effect of each slot. Note the side slip effect in Figure 5h at  $\alpha \geq 30^\circ$ . At  $\beta = +0.4^\circ$  (Figure 5g), all slots generate positive pitching moment increments. But, at  $\beta = +10.4^\circ$  (Figure 5h), a sudden slope reversal is indicated with all slots either generating negative pitching moment increments or indicating at higher angles of attack ( $\alpha > 34^\circ$ ) would generate negative increments.

### Tangential Slot Blowing

Tangential slot blowing is illustrated in Figure 6 below. Negative yawing moment increments (direction towards the blowing side) were generated

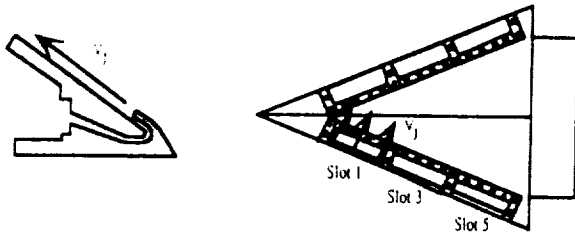


Figure 6 Tangential Slot Blowing

from all tangential slots examined (Figure 6a, b, and c) which are independent of slot length, position, mass flow, angle of attack and sideslip. In Figures 6a and 6b, as the slot length is increased or the slot is moved aft, the ability of the slot to generate incremental yawing moments decreases independently of sideslip with slot 1 generating the largest increment and slot 1-3-5 the least. In Figure 6a ( $\beta = +0.4^\circ$ ) at  $\alpha = 26^\circ$ , observe the slot position effect when moving the slot from slot 1 to slot 3. Moving the slot aft has the same effect as increasing the slot length; it diminishes the magnitude of yawing moment increments. No strong sideslip effects are noted except the slots generate larger yawing moment increments than at no sideslip. This again is in part due to the leeward forebody planform angle increasing commensurate with sideslip. Observe in Figures 6a through 6c how all slots exhibit a low angle of attack ( $\alpha < 15^\circ$ ) effectiveness at generating incremental yawing moments. This low angle of attack effectiveness is not necessarily due to vortex manipulation but attributed to the increased circulation across the forebody surface due to the jet sheet exiting from the slot thereby generating circulation induced forebody forces and moments. Since slot 1 appears to offer the largest yawing moment increments over a larger angle of attack range, only its  $C_{\mu}$  effects (Figure 6c) are shown. As  $C_{\mu}$  is increased, the incremental yawing moment generation of slot 1 also increases.

Regardless of mass flow, slot length, position, and sideslip, negative incremental side forces (direction towards the blowing side) are typically observed for all slots examined (Figures 6e through 6h). It is observed that slot 1 produces larger negative side force increments over a larger angle of attack range than any other slot length or position or sideslip. In Figures 6d and 6e, as the slot length is increased, the angle of attack at which the maximum incremental side force occurs decreases. Also, observe in Figures 6e through 6h how all slots exhibit a low angle of attack ( $\alpha < 15^\circ$ ) effectiveness at generating incremental side forces. Since slot 1 offers the largest yawing moment increments over the largest angle of attack range, only its  $C_{\mu}$  effects (Figure 6g) are shown. As  $C_{\mu}$  is increased, the incremental side force generation of slot 1 also increases. Slot 1  $C_{\mu}$  effects at  $\beta = +10.4^\circ$  are shown in Figure 6h for constancy.

Negative (stabilizing) pitching moment increments are typically observed (Figure 6i and 6j)

from all slots examined regardless of sideslip and angle of attack with the exception of slot 1-3 at  $\beta = +0.4^\circ$  and  $\alpha \geq 30^\circ$ . Observe the sideslip effects at  $\alpha > 26^\circ$ . A strong slope reversal is indicated in the  $\beta = +0.4^\circ$  (with the exception of slot 1) but not in the  $\beta = +10.4^\circ$  data.

### Tangential Blowing versus F-16C Rudder Deflection

In Figures 7a and 7b, a comparison using slot 1 is made between the three blowing concepts, outward ( $C_{\mu} = 0.22$ ), downward ( $C_{\mu} = 0.11$ ), and tangential ( $C_{\mu} = 0.22$ ) and an F-16C<sup>6</sup> rudder deflected  $+30^\circ$  at generating yawing moment and side force increments. As seen in Figures 7a and 7b, none of the chine blowing concepts surpassed the yawing and side force increment generation capability of the F-16C rudder at maximum rudder deflection. However, FVC on a chined forebody can augment (even at low angles of attack) the rudder in yawing moment and side force generation which could result in reduced vertical tail size.

### Chine Forebody Blowing versus Rounded Forebody Blowing

In Figure 8, a comparison is made of FLAC's tangential slot 1, chine forebody blowing to an F-18 slot blowing<sup>7</sup>, F-16 slot blowing<sup>8</sup>, and X-29 jet blowing<sup>9</sup>. This comparison is accomplished only to observe trends and rough orders of magnitudes between the two types of forebodies and slot and jet blowing.

As indicated in Figure 8, tangential slot blowing from a chined forebody is apparently going to require significantly more energy (mass flow) to generate comparable yawing moment increments compared to the rounded forebody blowing. As noted in the chine blowing section, the chine generated vortices have a stable separation point and are resistant to manipulation. Whereas the rounded forebodies' vortex separation points are unstable and suitable to manipulations by small disturbances that can result in the generation of large asymmetric forces and moments. However, at high angles of attack, the forebody vortex goes off body where the tangential jet sheet is well underneath that vortex thereby reducing its capability of manipulating it. To possibly increase the high angle of attack effectiveness of chine blowing, placing a slot perpendicular to the chine line near the forebody apex or using discrete jet blowing that was used on the X-29 flight test might manipulate the off body vortex<sup>10</sup>. Also note at  $\alpha < 15^\circ$ , how the chine blowing ( $C_{\mu} = 0.022$ ) offers low angle of attack performance while the rounded type forebodies apparently do not.

### Conclusions and Recommendations

Three different pneumatic slot concepts blowing at or near a chined forebody edge using three

different fluid mechanisms to achieve asymmetric forces and moments were evaluated. Those three pneumatic concepts were outward, downward and tangential blowing that used vortex displacement, fluidic dam, and entrainment respectively, as fluid mechanism to generate forces and moments. Effects examined were length, position, mass flow, and sideslip. Comparisons were made of tangential slot blowing to a fully deflected F16C rudder and chine forebody slot blowing to rounded forebody jet and slot blowing.

The outward and downward slot blowing typically generated yawing moments and side forces in a direction opposite to the blowing side where tangential slot blowing typically generated yawing moments and side forces in the direction of the blowing side. Outward and tangential slot blowing exhibited low angle of attack effectiveness while the downward blowing did not. Positioning the slot to the most forward position (slot 1) on the forebody typically offered the greatest force and moment generation regardless of slot type (outward, downward, or tangential). Also, increasing the slot length or moving the slot position aft typically degraded slot performance at generating forces and moments. Tangential blowing at slot 1 typically was the best slot concept, position, and length evaluated. Of the three fluid mechanisms investigated, entrainment (tangential blowing) offered the best promise of generating larger asymmetric yawing moments and side forces, generating negative (stabilizing) pitching moment increments, and providing low angle of attack performance. Tangential slot blowing did not out perform the maximum rudder deflection of an F-16, but could be used to augment the rudder, particularly at low angles of attack, thereby offering the possibility of reducing the vertical tail size. Chined forebody slot blowing appears to require greater energy (mass flow) to acquire the same levels of increments when compared to non-chined forebody blowing. Further investigation into chined blowing can be in areas of evaluating the effects on lateral/directional control using jets in lieu of slots. Placing slots near the forebody apex oriented perpendicular to the chine edge for high angle of attack effectiveness. Also, forebody fineness ratio (moment arm), forebody cross sectional shape, and the chine included angle are independent variables that have significant impact on the magnitudes of the forces and moments generated by the forebody. The effects of these independent variables certainly warrant further investigations.

#### Acknowledgments

This experimental investigation would not have been possible without help from Mr. Kevin Langan, Wright-Patterson AFB, Mr. Kevin James, Sterling Software NASA-Ames, 7x10 wind tunnel staff,

Jennifer and David Alexander, Dayton, Ohio, and Mr. Gino Welcelean and Lee Woolridge Micro Craft Inc., Tullahoma, Tn.

#### References

- 1) Malcolm, G., "Forebody Vortex Control - A Progress Review", AIAA Paper 93-3540, August 1993.
- 2) Walchli, L.A., Ryan, R.J., Smith, W.R., X-29 High Angle-of-Attack Flight Test Program, WL-TR-93-3003, January 1992.
- 3) Ralston, J., Avent, J., Dickes, E., A Feasibility Study of Forebody Vortex Control on a Chined Forebody, WL-93-3027, January 1993.
- 4) Fluid Meters, Their Theory and Application, The American Society of Mechanical Engineers, 6th edition, 1971.
- 5) Thermodynamics of Incompressible and Compressible Fluid Flow, AIR1168/1, SAE Aerospace Applied Thermodynamics Manual, 31 March 1990.
- 6) Century Computing, Inc., Simulation Rapid-Prototyping Facility, User's Manual, December 23, 1992.
- 7) Kramer, B., Suarez, C., Malcom, G., James, K., "Forebody Vortex Control with Jet and Slot Blowing on an F/A18", AIAA Paper 93-3449, August 1993.
- 8) LeMay, S.P., Sewall, W.G., Henderson, J.F., "Forebody Vortex Control on the F-16C using Tangential Slot and Jet Nozzle Blowing", AIAA Paper 92-0019, January 1992.
- 9) Guyton, R.W., Maerki, G., "X-29 Forebody Jet Blowing", AIAA Paper 92-0017, January 1992.
- 10) Private communication with Dr. Lawrence Walchli, Wright-Patterson AFB, Ohio, 7 April 1994, (brief meeting)

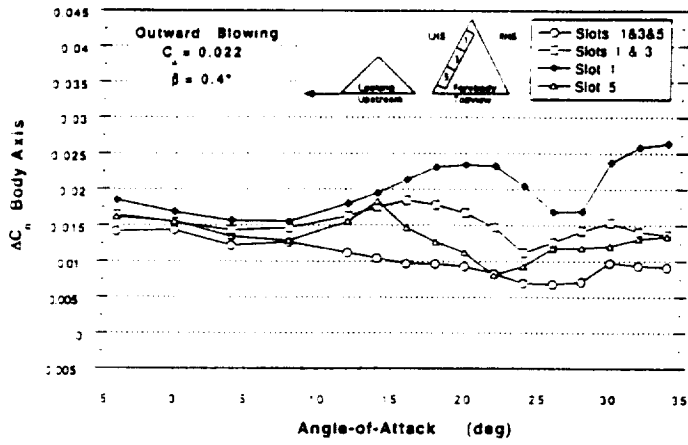


Figure 4a Outward Blowing,  $C_{\mu} = 0.022$ ,  $\beta = 0.4^{\circ}$   
Slot Effect,  $\Delta C_n$

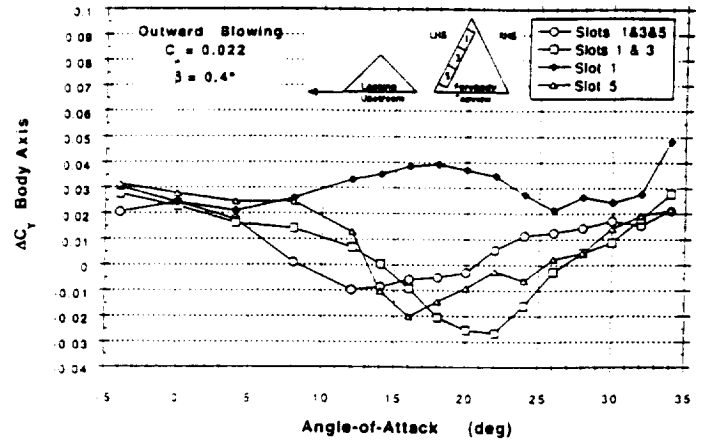


Figure 4d Outward Blowing,  $C_{\mu} = 0.022$ ,  $\beta = 0.4^{\circ}$   
Slot Effect,  $\Delta C_{\gamma}$

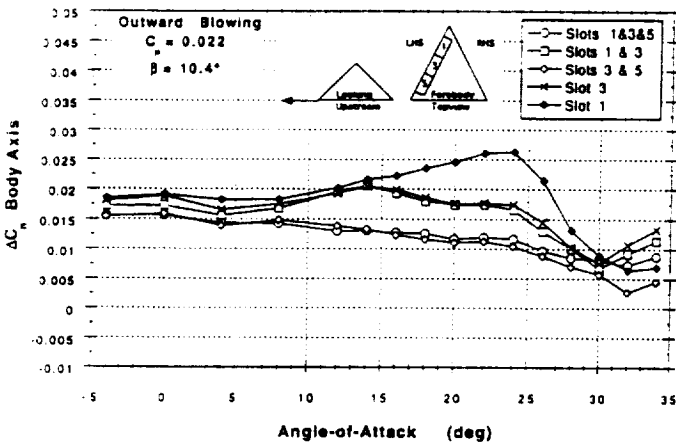


Figure 4b Outward Blowing,  $C_{\mu} = 0.022$ ,  $\beta = 10.4^{\circ}$   
Slot Effect,  $\Delta C_n$

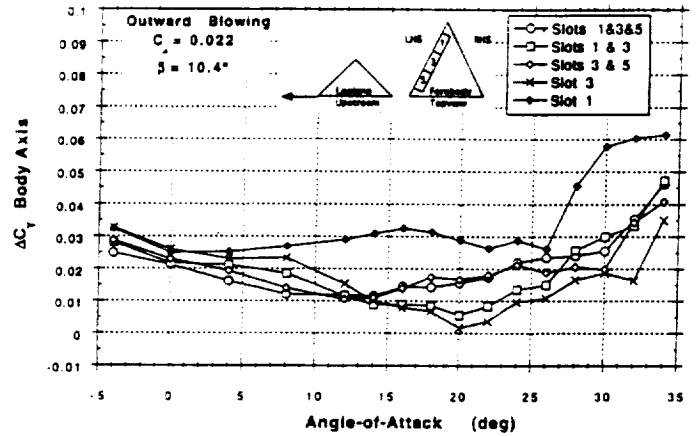


Figure 4e Outward Blowing,  $C_{\mu} = 0.022$ ,  $\beta = 10.4^{\circ}$   
Slot Effect,  $\Delta C_{\gamma}$

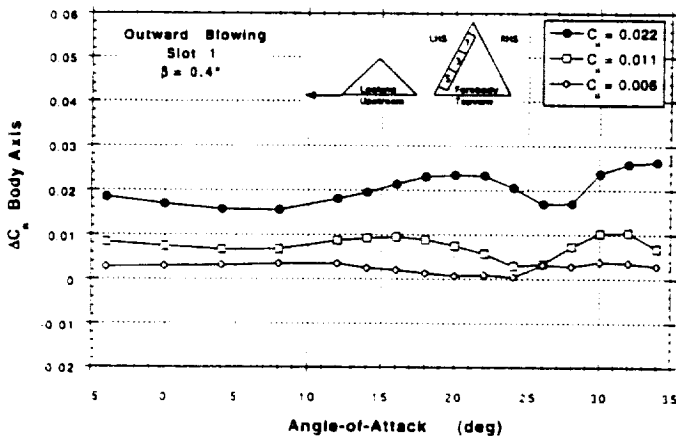


Figure 4c Outward Blowing, Slot 1,  $\beta = 0.4^{\circ}$   
 $C_{\mu}$  Effect,  $\Delta C_n$

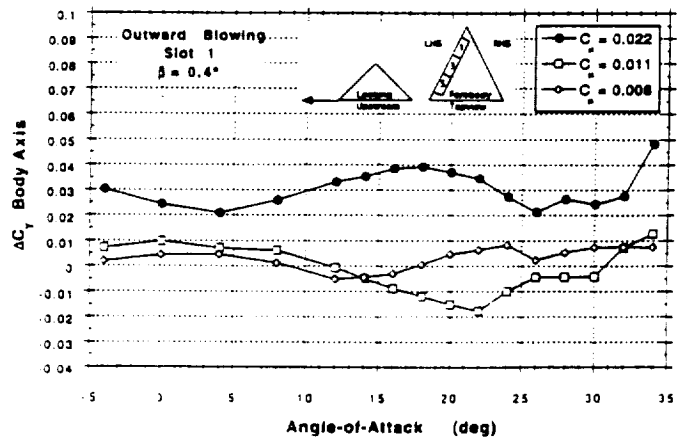


Figure 4f Outward Blowing, Slot 1,  $\beta = 0.4^{\circ}$   
 $C_{\mu}$  Effect,  $\Delta C_{\gamma}$

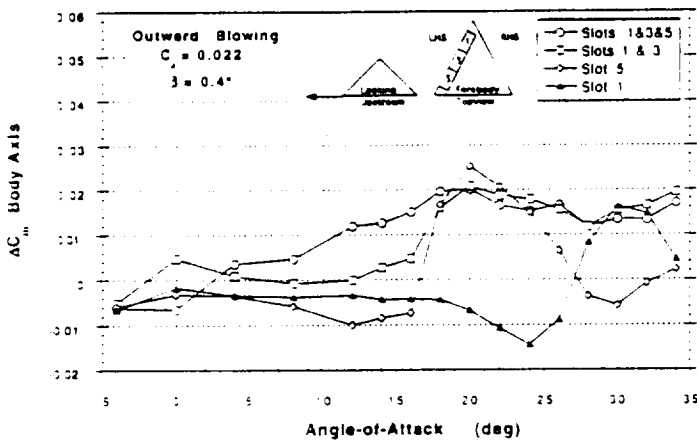


Figure 4g Outward Blowing,  $C_\mu = 0.022$ ,  $\beta = 0.4^\circ$   
Slot Effect,  $\Delta C_m$

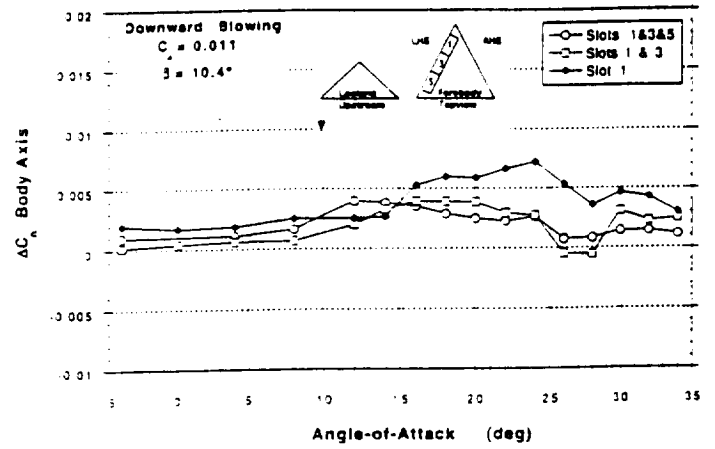


Figure 5b Downward Blowing,  $C_\mu = 0.011$ ,  $\beta = 10.4^\circ$   
Slot Effect,  $\Delta C_n$

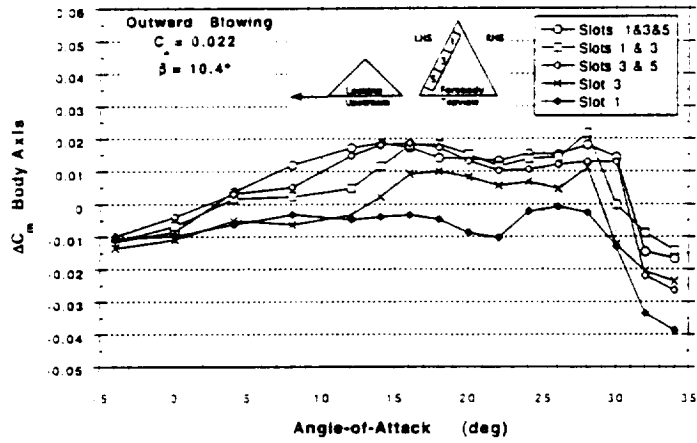


Figure 4h Outward Blowing,  $C_\mu = 0.022$ ,  $\beta = 10.4^\circ$   
Slot Effect,  $\Delta C_m$

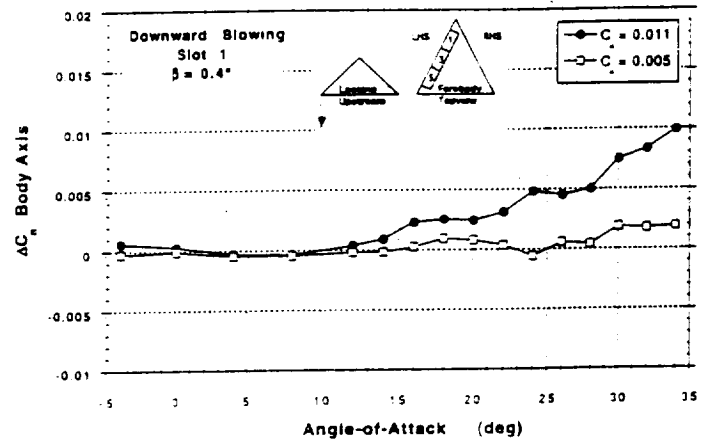


Figure 5c Downward Blowing, Slot 1,  $\beta = 0.4^\circ$   
 $C_\mu$  Effect,  $\Delta C_n$

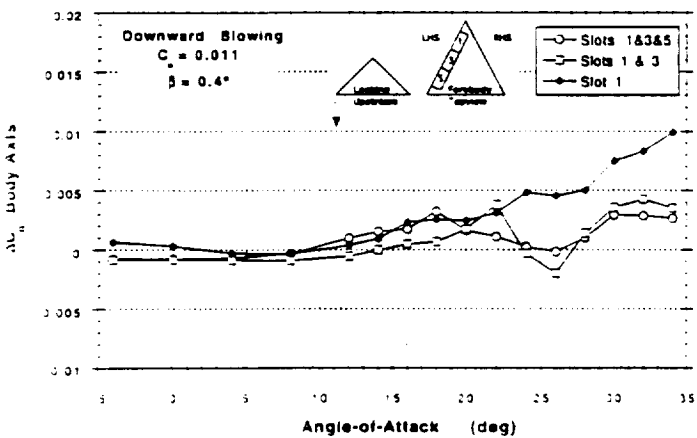


Figure 5a Downward Blowing,  $C_\mu = 0.011$ ,  $\beta = 0.4^\circ$   
Slot Effect,  $\Delta C_n$

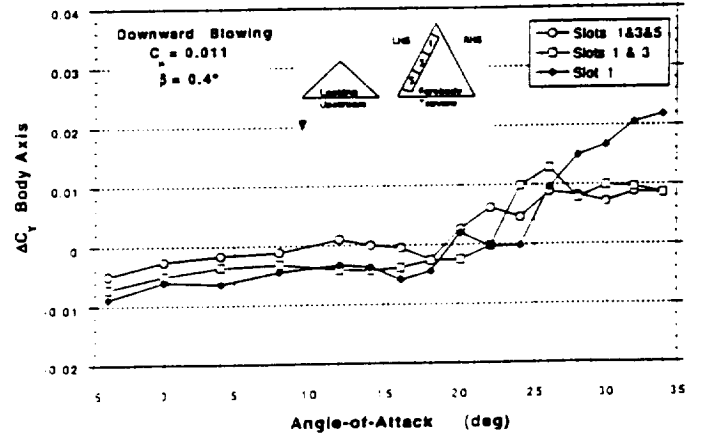


Figure 5d Downward Blowing,  $C_\mu = 0.011$ ,  $\beta = 0.4^\circ$   
Slot Effect,  $\Delta C_y$

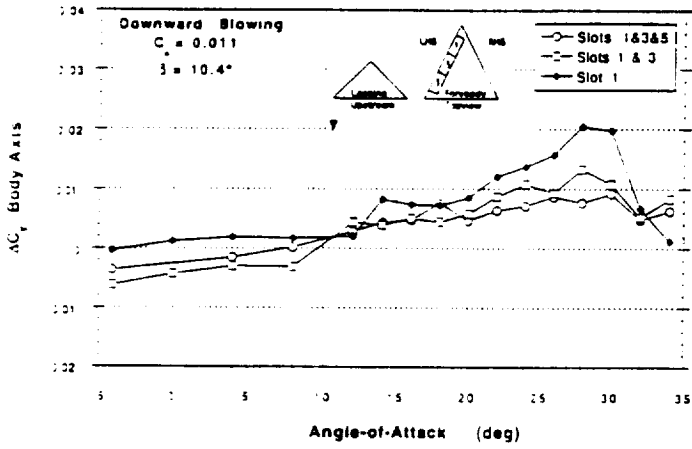


Figure 5e Downward Blowing,  $C_{\mu} = 0.011$ ,  $\beta = 10.4^{\circ}$   
Slot Effect,  $\Delta C_{\gamma}$

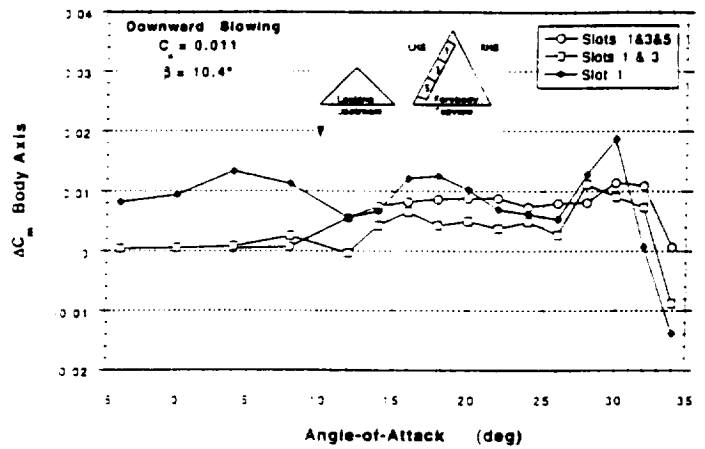


Figure 5h Downward Blowing,  $C_{\mu} = 0.011$ ,  $\beta = 10.4^{\circ}$   
Slot Effect,  $\Delta C_m$

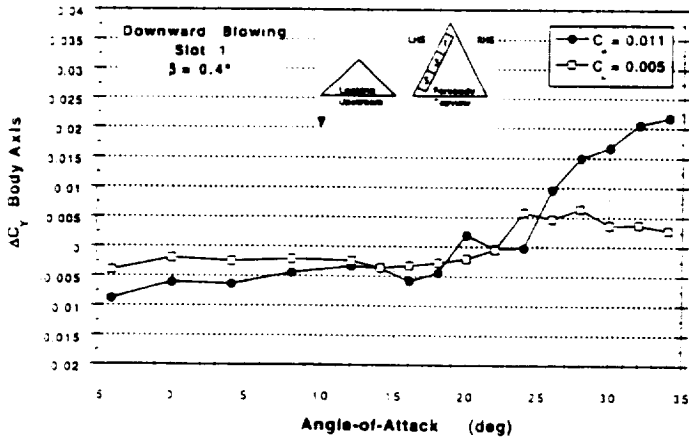


Figure 5f Downward Blowing, Slot 1,  $\beta = 0.4^{\circ}$   
 $C_{\mu}$  Effect,  $\Delta C_{\gamma}$

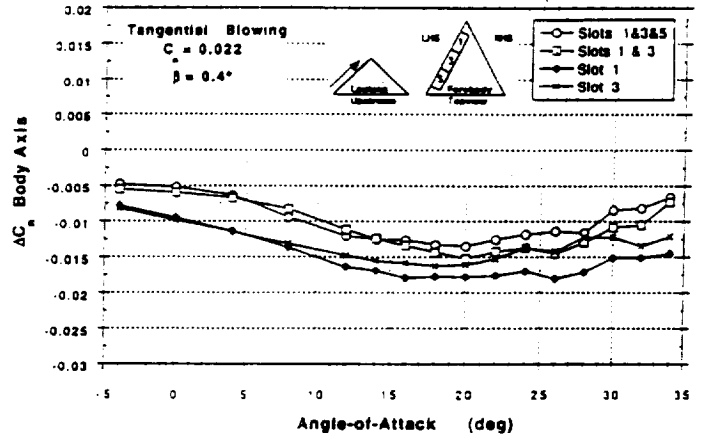


Figure 6a Tangential Blowing,  $C_{\mu} = 0.022$ ,  $\beta = 0.4^{\circ}$   
Slot Effect,  $\Delta C_n$

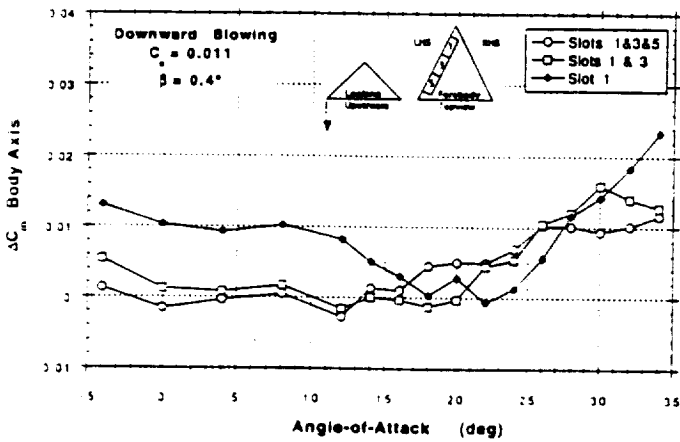


Figure 5g Downward Blowing,  $C_{\mu} = 0.011$ ,  $\beta = 0.4^{\circ}$   
Slot Effect,  $\Delta C_m$

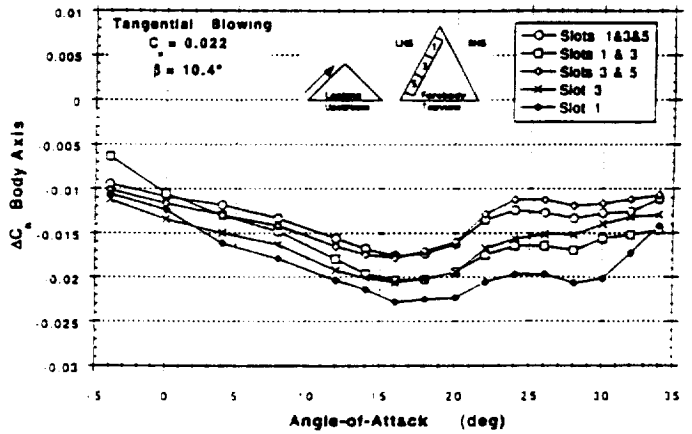


Figure 6b Tangential Blowing,  $C_{\mu} = 0.022$ ,  $\beta = 10.4^{\circ}$   
Slot Effect,  $\Delta C_n$

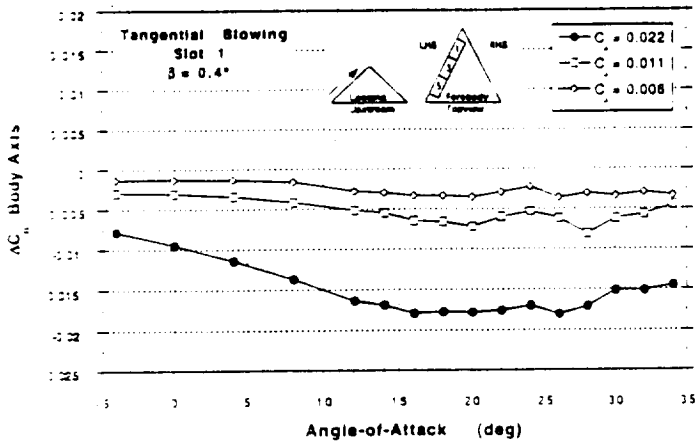


Figure 6c Tangential Blowing, Slot 1,  $\beta = 0.4^\circ$   
 $C_{\mu}$  Effect,  $\Delta C_n$

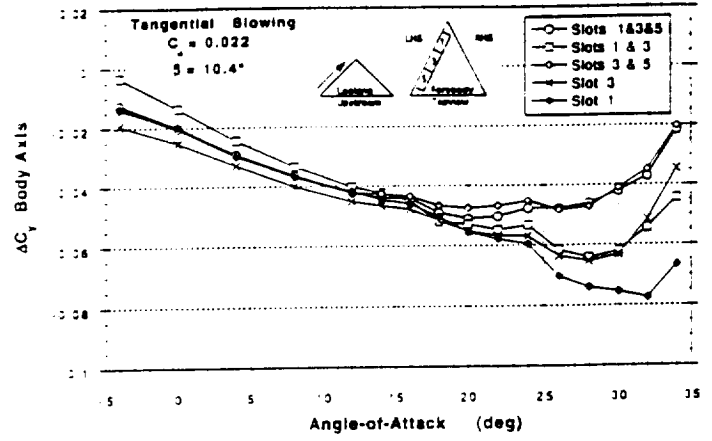


Figure 6f Tangential Blowing,  $C_{\mu} = 0.022$ ,  $\beta = 10.4^\circ$   
 Slot Effect,  $\Delta C_Y$

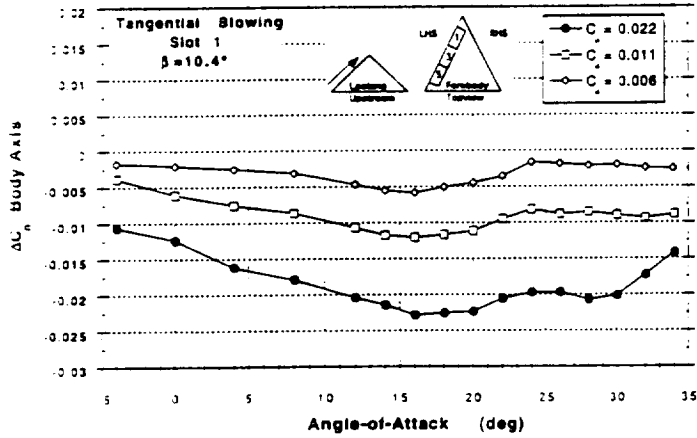


Figure 6d Tangential Blowing, Slot 1,  $\beta = 10.4^\circ$   
 $C_{\mu}$  Effect,  $\Delta C_n$

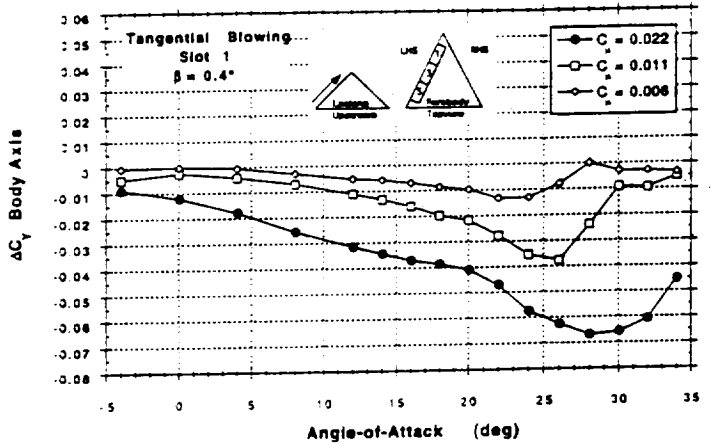


Figure 6g Tangential Blowing, Slot 1,  $\beta = 0.4^\circ$   
 $C_{\mu}$  Effect,  $\Delta C_Y$

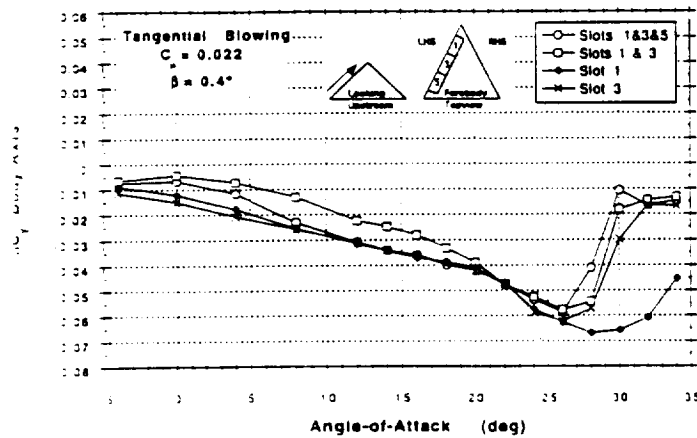


Figure 6e Tangential Blowing,  $C_{\mu} = 0.022$ ,  $\beta = 0.4^\circ$   
 Slot Effect,  $\Delta C_Y$

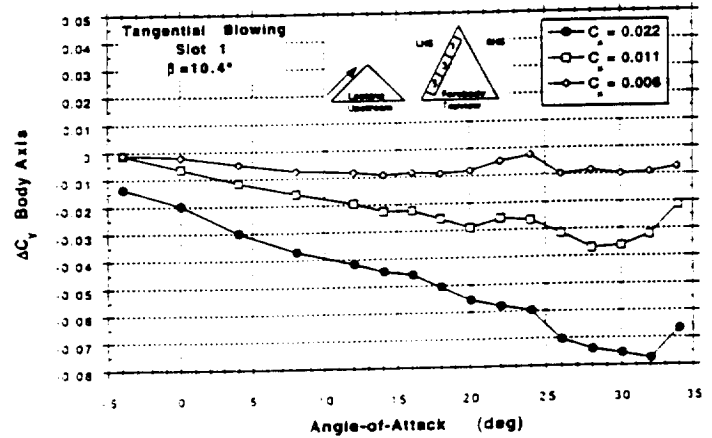


Figure 6h Tangential Blowing, Slot 1,  $\beta = 10.4^\circ$   
 $C_{\mu}$  Effect,  $\Delta C_Y$

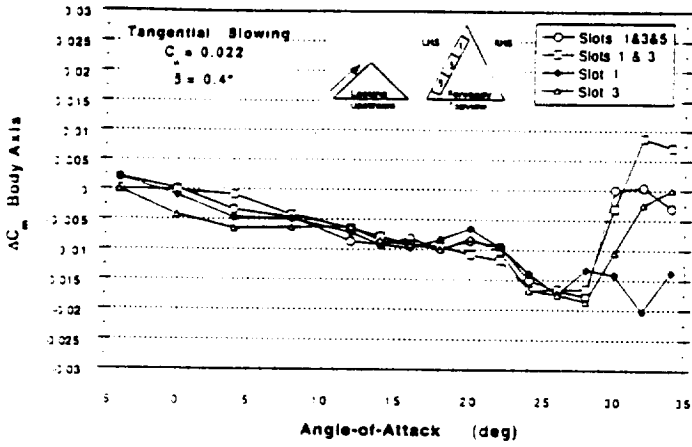


Figure 6i Tangential Blowing,  $C_{\mu} = 0.022$ ,  $\beta = 0.4^{\circ}$   
Slot Effect,  $\Delta C_m$

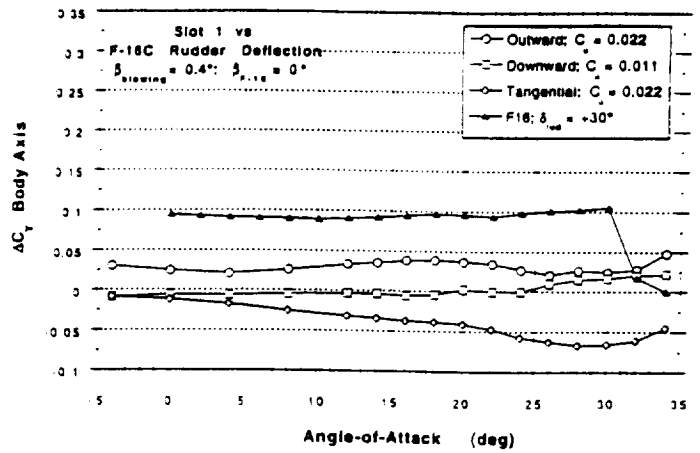


Figure 7b Tangential Blowing versus F-16 Rudder  
Deflection,  $\delta_{rud} = +30^{\circ}$ ,  $C_{\mu} = 0.022$ ,  $\Delta C_y$

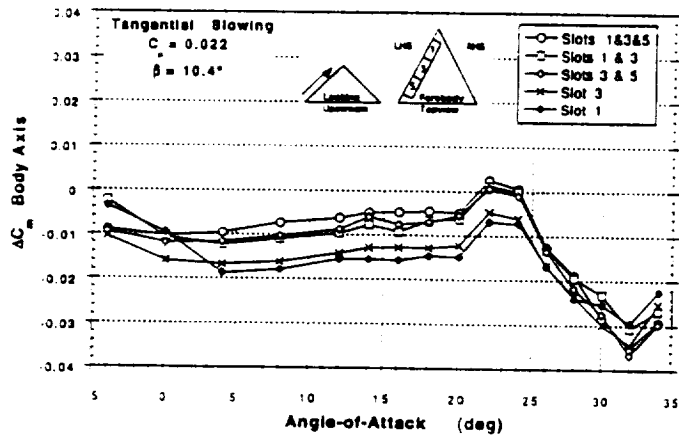


Figure 6j Tangential Blowing,  $C_{\mu} = 0.022$ ,  $\beta = 10.4^{\circ}$   
Slot Effect,  $\Delta C_m$

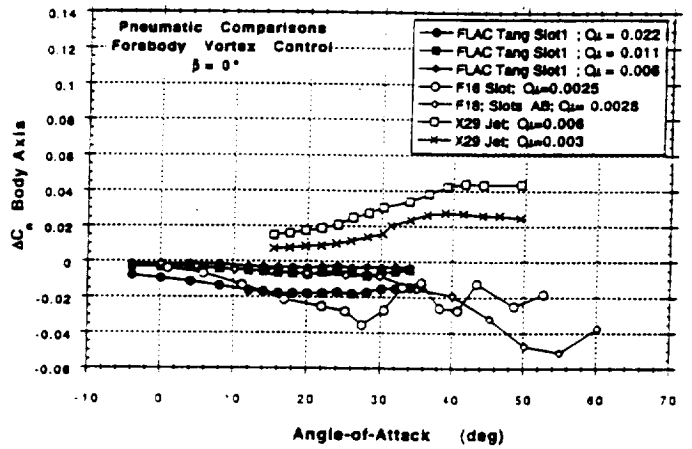


Figure 8 Pneumatic Comparisons,  $\beta = 0^{\circ}$

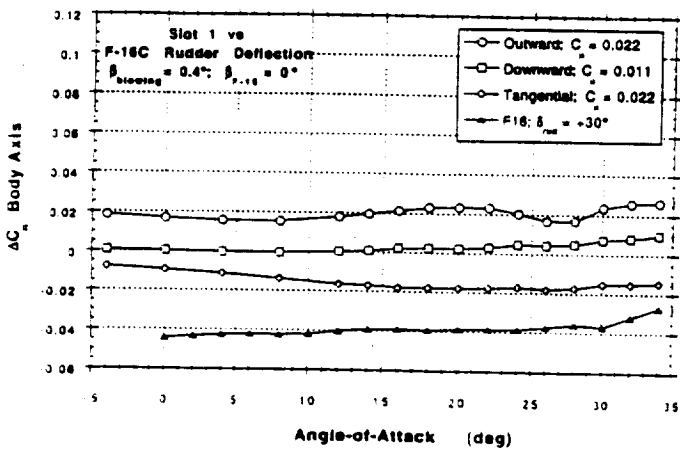


Figure 7a Tangential Blowing versus F-16 Rudder  
Deflection,  $\delta_{rud} = +30^{\circ}$ ,  $C_{\mu} = 0.022$ ,  $\Delta C_n$